

X-ray photoelectron spectroscopy of $\text{CeO}_2\text{--Na}_2\text{O--SiO}_2$ glasses

A. Mekki*

Department of Physics, King Fahd University of Petroleum and Minerals, Dhahran 31261, Saudi Arabia

Received 27 June 2004; received in revised form 8 September 2004; accepted 8 September 2004

Available online 12 October 2004

Abstract

A series of $(\text{CeO}_2)_x\text{--}(\text{Na}_2\text{O})_{0.3}\text{--}(\text{SiO}_2)_{(0.7-x)}$ glasses, where $0.025 \leq x \leq 0.075$, have been synthesized and investigated by mean of X-ray photoelectron spectroscopy (XPS). The Ce 3d spin-orbit doublet was curve fitted in order to quantify the proportions of each cerium oxidation state in these glasses. It was found that Ce ions are predominantly in the Ce(III) state in glasses with compositions $x \leq 0.075$, while mixed Ce valences were found in the glass with composition $x = 0.10$. The O 1s spectra have also been curve fitted with two components, one from bridging oxygen (BO) and the other from non-bridging oxygen atoms (NBO). The measured number of NBO, based on the fact that only oxygen atoms in the site Si--O--Na^+ contribute to the NBO peak, was found to be constant at $\sim 35\%$ for all samples, in good agreement with the value calculated from the glass composition and inductively coupled plasma (ICP) suggesting that Ce ions enter the network as a glass intermediate. The thermal measurements done on these glasses agree well with the XPS findings.

© 2004 Elsevier B.V. All rights reserved.

Keywords: XPS; Ce 3d; O 1s; Bridging oxygen; Non-bridging oxygen; Rare earth oxide glasses

1. Introduction

Rare earth ions doped materials are good candidates for optical, lasing as well as magnetic applications [1,2]. Cerium doped crystalline materials have shown interest both academically and industrially because of their electrical, optical, catalytic and magnetic properties [3–6]. Oxide glasses containing cerium have been recently investigated for their optical and lasing properties [7–9]. Several optical techniques have been used to investigate these materials [10,11]. However, very few systematic work has been done to study the structural and physical properties of cerium doped oxide glasses especially when large concentrations (more than 2 mol%) of CeO_2 are introduced in the glass network [12].

X-ray photoelectron spectroscopy (XPS) is a well-established surface analytical technique used in glass science and technology to study the elemental surface composition, the nature of the oxygen bonding and the oxidation state of the cations in glasses [13]. Recently, the technique has been

used to investigate the structural properties of Pr_2O_3 ions in sodium silicate glasses [14]. From the Pr 3d core level spectra we established that Pr ions exist in the Pr(III) state only, while the O 1s core spectra were decomposed into bridging oxygen (BO) and non-bridging oxygen (NBO) atoms. The introduction of Pr ions in the glass network seemed to increase the number of NBO atoms indicating that Pr enters the glass network as a glass modifier. The physical properties measurements and the XPS findings were in good agreement.

To the best of our knowledge, there are only two published XPS works on glasses containing Ce ions. The first study was done by Harrison et al. [15] who investigated the interaction of Ce ions and glass surfaces. They found that Ce undergoes no change in oxidation state on surface adsorption. Their work did not deal with structural properties of Ce doped glasses. In a very recent work [16], the authors used XPS to investigate the oxidation state of Ce ions during leaching of CeYSiAlO glass. They found, through curve fitting of the Ce 3d spectrum of the glass, that Ce ions exist in both Ce(III) and Ce(IV) oxidation states in that glass sample after leaching.

In this paper, we extend our previous work on the sodium silicate glasses containing rare earth oxide Pr_2O_3 by present-

* Tel.: +966 3 860 4292; fax: +966 3 860 2293.

E-mail address: akmekki@kfupm.edu.sa.

ing the first study of the structural and physical properties of CeO₂ sodium silicate glasses. The objective of this work is to identify the structural role of Ce ions which will be done through the analysis the O 1s core level spectra. Also we would like to know the oxidation states of Ce ions in these glasses by analyzing the Ce 3d core level spectra. The results of the XPS study and the thermal and physical properties will be compared.

2. Experimental details

2.1. Glass preparation

The glass samples were prepared using commercially available, analytical grade powders of CeO₂, Na₂CO₃ (for Na₂O) and SiO₂. Calculated amounts of these powders were mixed and melted in 95%Pt/5%Rh crucibles at 1400 °C for two hours. After quenching the melt quickly, the glass was crushed and remelted at the same temperature to ensure homogeneity of the product. The final melt was then cast into preshaped, graphite-coated steel moulds yielding bar specimens with dimensions 6 mm in diameter and 2 cm in length. After casting, the specimens were transferred to another furnace maintained at 50 °C below the glass transition temperature T_g , determined from the differential thermal analysis (DTA), for two hours and then cooled to room temperature at a rate of 30 °C/hour. X-ray powder diffraction analysis indicated that the glasses thus formed were amorphous within the detection limit of the technique. After preparation, the samples were stored in a desiccator. Chemical compositions were determined by inductively coupled plasma (ICP), emission spectroscopy. Each composition was analyzed at least twice and the estimated relative uncertainty in the composition derived from this technique was estimated to be ±5%. Table 1 lists the batch and the analyzed glass compositions.

2.2. Measurement of physical properties

Several physical properties of each glass sample were measured. Glass transition temperatures (T_g) were measured using DTA (heating rate 10 °C/min), and thermal expansion coefficients (α) were determined in the temperature range from room temperature to the softening point of each glass using dilatometry and a heating rate of 1 K/min. The thermal

Table 1

Nominal and actual composition (molar fraction) of various cerium doped sodium silicate glasses

| Nominal | | | Actual (from ICP) | | |
|------------------|-------------------|------------------|-------------------|-------------------|------------------|
| CeO ₂ | Na ₂ O | SiO ₂ | CeO ₂ | Na ₂ O | SiO ₂ |
| 0.025 | 0.30 | 0.675 | 0.024 | 0.297 | 0.679 |
| 0.050 | 0.30 | 0.650 | 0.049 | 0.298 | 0.653 |
| 0.075 | 0.30 | 0.625 | 0.079 | 0.305 | 0.616 |
| 0.10 | 0.30 | 0.60 | 0.098 | 0.308 | 0.594 |

The relative uncertainty in the ICP results is ±5%.

expansion coefficient was measured relative to that of silica with a certain correction factor. The density of each glass was also measured using Archimedes' principle and each sample was weighed both in air and in degassed, distilled water.

2.3. XPS measurements

Photoelectron spectra from the C 1s, O 1s, Ce 3d, Na 1s and Si 2p core levels were recorded with V.G. Scientific ESCALAB MkII spectrometer using a non-monochromatic Al source (K_{α} , 1486.6 eV). The output power was 130 W. The binding energy of the spectrometer was calibrated by several reference lines (Cu 2p_{3/2} = 932.67 eV, Cu 3p_{3/2} = 74.9 eV and Au 4f_{7/2} = 83.98 eV). The pass energy of the electron analyzer was fixed at 10 eV. The energy resolution was about 1.0 eV. For the XPS measurements, a glass rod from each composition was subsequently fractured in ultra high vacuum (UHV), where the base pressure in the analysis chamber was better than 2×10^{-10} mbar. The glass bars were notched to guide the fracture yielding flat, uncontaminated surfaces.

Fracturing in UHV is regarded to be the optimum method to observe the bulk electronic structures of the glass samples. Any other surface treatment (such as ion bombardment) may cause changes in surface composition and chemical state of the glass, especially the alkali ion distribution. For consistency, all binding energies are reported with reference to the C 1s transition at 284.6 eV ± 0.2 eV. This is a peak arising from a minor quantity of hydrocarbon contaminants present in the vacuum and is generally accepted to be independent of the chemical state of the sample under investigation. All of the spectra presented in this paper have been corrected for the charging effect. The O 1s and Ce 3d spectra were fitted with the weighted sum of two Gaussian–Lorentzian curves representing the bridging and non-bridging oxygen contributions, and the possible cerium valencies, respectively. The Lorentzian component of the fitted spectrum arises from the natural peak shape, while the Gaussian component represents the instrumental broadening contribution to the spectrum. A non-linear, least square fitting algorithm was used to find each best fit solution. Satellites Al $K_{\alpha 3,4}$ were subtracted before any spectral analysis of the Ce 3d spectra was done. The BO and NBO atomic ratio and the Ce(III)/Ce(IV) ratio were determined from the ratio of the areas under the respective peak. Several samples were analyzed in this manner and the overall accuracy in determining the peak position and chemical shift was smaller than 0.2 eV. The quantitative oxygen bonding results and cerium redox analysis were reproducible within ±5% and ±10%, respectively.

3. Results and discussion

3.1. Physical properties

The nominal and analyzed compositions of the glasses studied here are given in Table 1. The variations with com-

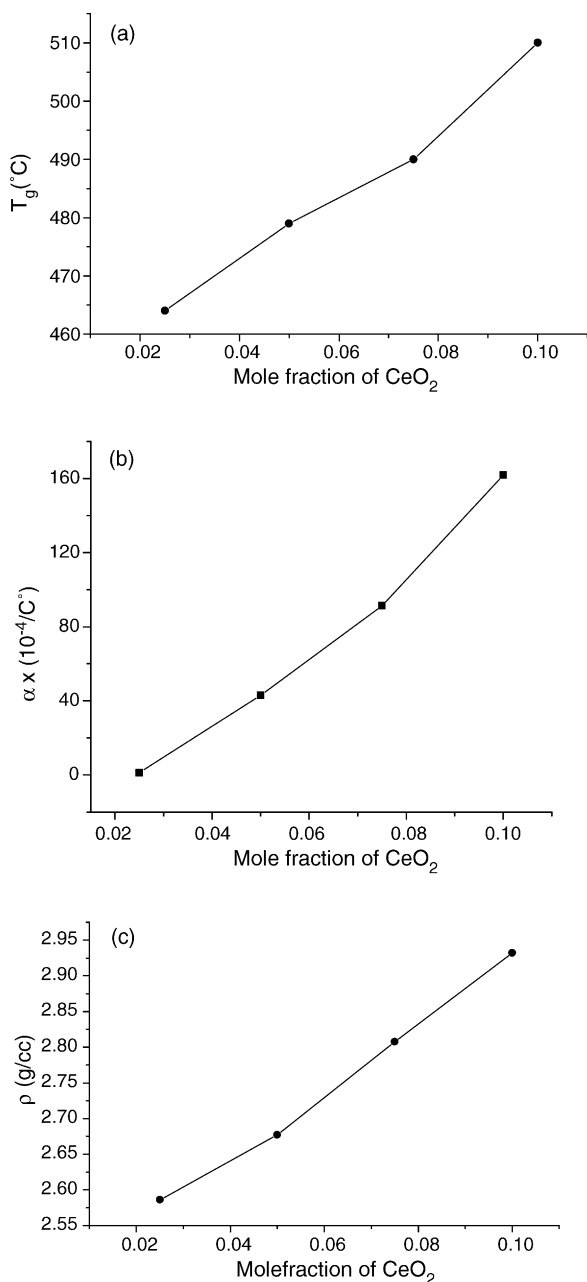


Fig. 1. Variations in (a) the glass transition temperature (T_g), (b) the linear thermal expansion coefficient (α) and (c) the density (ρ) as a function of CeO₂ content in the glass.

position of glass transition temperature (T_g), linear thermal expansion coefficient (α) and density (ρ) of the cerium doped glasses are shown in Fig. 1 a–c as a function of Ce content. The ICP analysis shows that there is not much difference between the batch and the actual composition of the samples. The glass transition temperature shows an almost linear increase from $\sim 460^\circ\text{C}$ for $x=0.025$ to $\sim 510^\circ\text{C}$ for $x=0.10$. The increase in T_g indicates a strengthening of the glass network upon introducing CeO₂ in the glass. The variation of the thermal expansion coefficient shows similar trend as do the glass transition temperature and the density with values varying from

$\sim 1.319 \times 10^{-4}/^\circ\text{C}$ for $x=0.025$ to $\sim 161.75 \times 10^{-4}/^\circ\text{C}$ for $x=0.10$. This increase in α confirms the strengthening of the glass network suggested by the T_g data measurements. The density of the glass also shows a linear increase from $\sim 2.587\text{ g/cm}^3$ for $x=0.025$ to $\sim 2.932\text{ g/cm}^3$ for $x=0.10$. This increase of density is expected as the molar weight of Ce is much higher than that of Si. Therefore substituting Ce for Si would result in an increase in density of the glass.

3.2. XPS Spectra

3.2.1. Ce 3d spectra

The XPS analysis was used to determine the oxidation state of Ce ions in each glass sample. Fig. 2 shows the Ce 3d core level spectra for all the Ce doped glasses in the binding energy (BE) range 870–930 eV. Care was taken to keep the same experimental conditions throughout the analysis of each sample as reflected by the clear increase in the intensity of the Ce 3d core level spectra on going from $x=0.025$ to $x=0.10$. The peaks are broad and each spin-orbit component is composed of a doublet peak. The higher BE contribution to the doublet peak is more intense than the one at the lower BE for all four spectra. The Ce 3d core level spectra of the glasses are compared with those of the oxides of Ce(III)₂O₃ and Ce(IV)O₂ from references 16 and 17 [16,17]. Both Ce(III) and Ce(IV) show the 3d_{5/2} and 3d_{3/2} multiplet splitting, but for the latter, each component shows three peaks instead of two. In the case of Ce (IV) a peak is also observed at a BE of $\sim 916\text{ eV}$. This corresponds to the initial state of the tetravalent Ce (called “f⁰” configuration) that is not found in the initial state of trivalent Ce [16]. This peak at a BE of $\sim 916\text{ eV}$ is not observed for Ce(III) and it is thus possible to differentiate between the two oxidation states. As seen from Fig. 2, there is either a very small or no peak at a BE of $\sim 916\text{ eV}$ for the glass samples with compositions $x \leq 0.075$. However, there is a small peak at that BE for the $x=0.10$ glass sample indicating there is a mixture of Ce(III) and Ce(IV) ions in that sample. If we compare the intensity of the peak at a BE

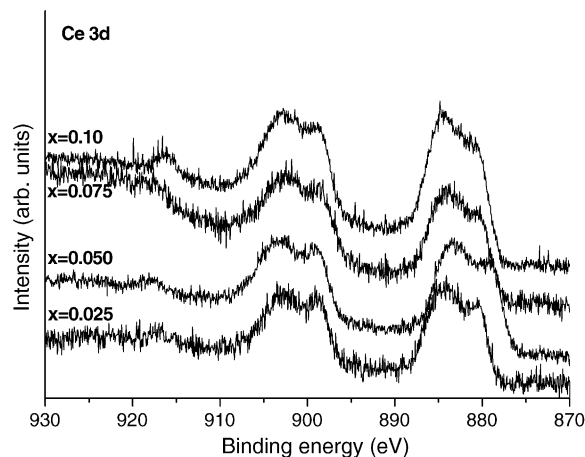


Fig. 2. Ce 3d photoemission core level spectra for the four glass samples showing the spin-orbit doublet Ce 3d_{3/2} and Ce 3d_{5/2}.

of 916 eV from the glass sample with composition $x=0.10$ with that of the Ce(IV)O₂ standard sample, we see that for the glass sample, the peak is too small indicating that the proportion of Ce(IV) ions compared to that of Ce(III) ions is small.

In order to quantify the two possible oxidations states of Ce ions in these glasses it is necessary to curve fit the Ce 3d_{5/2} and the Ce 3d_{3/2} spin-orbit doublet spectrum for each glass composition. Fig. 3a and b show such a fitting for the $x=0.05$ and the $x=0.10$ glass composition, respectively. The BE positions of the fitted components are chosen initially similar to those found in earlier work published on CeYSiAlO glass [16] and CeMnO catalyst [18]. The fitting program makes up to 1000 iterations and fixes the values of the BE 's reported

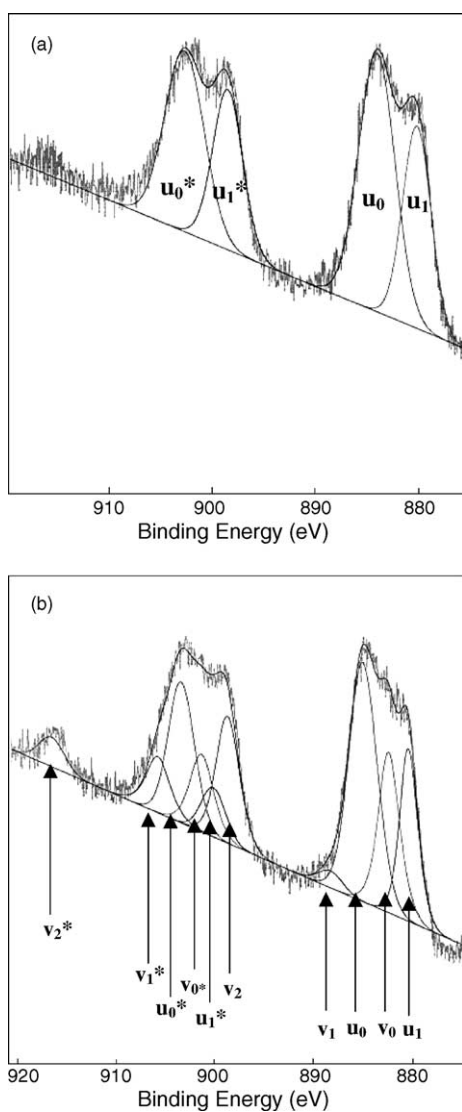


Fig. 3. (a) Ce 3d core level peak for the $x=0.05$ glass composition, curve fitted with four individual peaks (u lines) corresponding to contributions from Ce(III) ions only. (b) Ce 3d core level peaks for the $x=0.10$ glass composition curve fitted with ten individual peaks (u line) corresponding to contributions from Ce(III) ions and (v lines) corresponding to contributions from Ce(IV) ions.

Table 2

Binding energies of the fitted components of the Ce 3d_{5/2} due to Ce⁴⁺ ions and denoted v_0, v_1, v_2 , while those due to Ce³⁺ ions are denoted u_0 and u_1

| x | Ce 3d _{5/2} (eV) | ΔE (eV) |
|-------|---------------------------|-----------------|
| 0.025 | u_1 : 880.2 | 18.3 |
| | u_0 : 884.1 | 18.6 |
| 0.050 | u_1 : 880.2 | 18.3 |
| | u_0 : 884.1 | 18.6 |
| 0.075 | u_1 : 880.1 | 18.4 |
| | u_0 : 884.0 | 18.7 |
| 0.10 | u_1 : 880.2 | 18.5 |
| | u_0 : 884.2 | 18.7 |
| | v_0 : 882.2 | 19.0 |
| | v_1 : 888.2 | 17.9 |
| | v_2 : 898.5 | 17.9 |

The BE are measured relative to C 1s (284.6 eV). The uncertainty in the peak position is ± 0.20 eV. ΔE represents the energy separation between the spin-orbit components.

in Table 2. As seen from Fig. 3a, the spectrum for the $x=0.05$ glass composition looks similar to the one for Ce₂(III)O₃ [16] and was therefore fitted with only four components as was done in previous work [16,18]. The assignment of the fitted peaks is similar to the one adopted by Burroughs et al. [19]. The peaks labeled u_0 and u_0^* and having BE's of ~ 884 and ~ 903 eV, respectively, are due to 3d⁹4f¹ photoemission final state. The satellite peaks u_1 and u_1^* with a BE of ~ 880 and ~ 899 eV, respectively, are caused by the ligand to metal charge transfer by the primary photoionization process and are "shakedown" satellite features. These four contributions to the Ce 3d spectrum are due to Ce(III) ions only [19]. The spectra for the $x=0.025$ and the $x=0.075$ glass compositions, not shown here, were also curve fitted with four contributions, taking into account the fact that only Ce(III) ions are present and are similar to the one shown in Fig. 3a. The spectrum for the glass composition $x=0.10$ has a small peak at a BE of ~ 916 eV indicating the presence of Ce(IV) as previously discussed. However, this peak is small compared to the one from pure Ce(IV)O₂ sample and therefore we expect the proportion of Ce(IV) ions in this sample to be small compared to that of Ce(III) ions for this glass composition. Fig. 3b shows the Ce 3d spectrum fitted with contribution from both Ce(III) and Ce(IV) ions. The number of peaks used (ten) and the choice of the BE position and the full width at half maximum (FWHM) of each fitted peak are consistent with previously published XPS works [16,18]. Also, for consistency, almost the same BE's and FWHM were used for the peaks u_0, u_1, u_0^* and u_1^* in fitting the Ce 3d spectra of the four glass compositions. The BE positions of the fitted contributing to the Ce 3d_{5/2} peak are reported in Table 2. They are in good agreement with values reported in the literature [16,18].

According to this study, only Ce(III) are present in the glass samples with composition $x \leq 0.075$, while the proportion of Ce(IV) to total cerium ions in the glass with composition $x=0.10$ was measured using the area ratio of the sum of the various peaks contributing from Ce(IV), and labeled, v_i , to the total area of the Ce 3d spectrum. The calculation leads to a ratio of $0.4 \pm 10\%$.

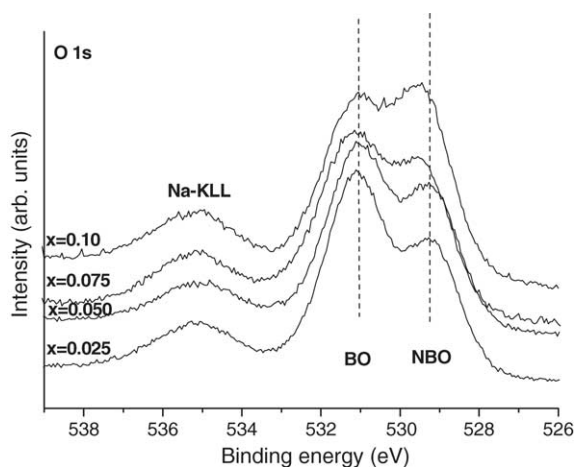


Fig. 4. O 1s core level spectra for the four CeNaSi glasses. The peak at a BE of ~ 535 eV is due to Na Auger transition and is not part of the O 1s spectrum. The lower BE transition is due to NBO atoms, while the higher BE peak is due to BO atoms.

3.2.2. O 1s spectra

The O 1s core spectra are very informative in terms of the structural role of cations in glasses [20]. Stacked core level O 1s spectra for the glass samples are shown in Fig. 4. As seen from the figure, there are three distinct peaks at BE of 529.5, 531.5 and 535 eV, the latter peak having a constant intensity is due to X-ray induced Na Auger electrons and is not associated with the O 1s. The intensity of the peak at the lower BE increases in intensity and its position seems to shift toward lower BE values with the increase in CeO_2 content in the glass (see Fig. 4). This peak corresponds to the contribution from non-bridging oxygen atoms, while the peak at a BE of 531.5 eV, having an almost constant BE regardless of the CeO_2 content, is due to contributions from bridging oxygen atoms. It is well known that SiO_2 is a glass former contributing BO atoms only, while Na_2O is a glass modifier. In fact, XPS has shown that, when a Na_2O molecule is introduced in a glass network 2 NBO are formed, disrupting the SiO_2 amorphous network [21]. However, there is no published research work on the structural role of CeO_2 in glass networks. In order to study the structural behavior of CeO_2 in sodium silicate glasses it is necessary to curve fit the O 1s spectra for each glass composition and see whether each CeO_2 molecule contributes NBO atoms and behaving as a glass modifier or BO atoms and behaving more like an intermediate. It is understood that CeO_2 cannot be a glass former. Fig. 5a and b show fitted O 1s spectra for the $x=0.025$ and the $x=0.075$ glass compositions, respectively. Each spectrum has been curve fitted with two contributions, one from NBO atoms at a BE of 529.5 eV and the other due to BO atoms at a BE of 531.5 eV. We tried to curve fit each O 1s core level peak with three components, one due to oxygen atoms in Si–O–Si configuration, a second due to oxygen atoms in Si–O–Ce configuration and the third due to oxygen atoms in Si–O– Na^+ configuration. Such a fitting would always converge to two components with zero FWHM for the second

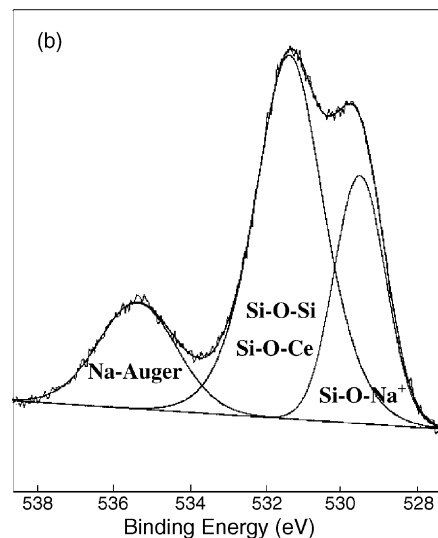
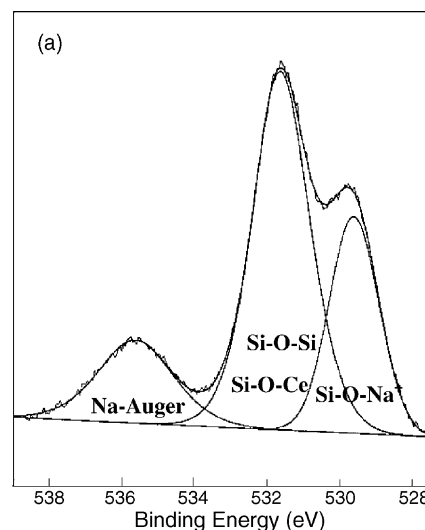


Fig. 5. O 1s core level spectra for the (a) $x=0.05$ glass composition and the (b) $x=0.075$ glass compositions, curve fitted with three components, one from oxygen atoms in the Si–O– Na^+ configuration, the other from oxygen atoms in the Si–O–Si and Si–O–Ce configuration. The third peak is a Na–Auger transition (a).

component. We did not impose any restriction on either BE or the FWHM of the two peak fit of the $x=0.025$ glass composition. The best fitting result (with the lowest χ^2 value) of the fitted spectrum for that composition are reported in Table 3. However, the fitting of the O 1s spectra for the other three glass compositions was done by imposing some constrained on the values of the BE and the FWHM of the NBO (or oxygen signal from Si–O– Na^+), using the values obtained from fitting the $x=0.025$ spectrum, while keeping those parameters corresponding to the BO signal free. The results of the fitting of the four spectra are summarized in Table 3. As we can see from the table, the BE and FWHM of the NBO contribution are almost constant for all four spectra. This resulted in an almost constant proportion of NBO ($\sim 35\%$). This can be understood by the fact that the Na_2O content

Table 3

Peak positions, FWHM, peak separation, and relative concentration of oxygen in Si–O–Na⁺ configuration resulting from the curve fitting of the O 1s core level for these glasses

| x | O 1s (eV) | | FWHM (eV) | | $\Delta E_{\text{BO-(Si-O-Na}^+)}$ | [Si–O–Na ⁺]/[TO] [*] % | |
|-------|----------------------|-------|----------------------|------|------------------------------------|---|------------|
| | Si–O–Na ⁺ | BO | Si–O–Na ⁺ | BO | | Measured | Calculated |
| 0.025 | 529.6 | 531.6 | 1.59 | 1.91 | 2.0 | 33.1 | 34.8 |
| 0.050 | 529.6 | 531.5 | 1.58 | 2.01 | 1.9 | 32.5 | 35.0 |
| 0.075 | 529.6 | 531.5 | 1.58 | 2.19 | 1.9 | 35.8 | 35.9 |
| 0.10 | 529.6 | 531.2 | 1.58 | 2.21 | 1.6 | 38.1 | 36.4 |

The experimental uncertainty is ± 0.2 eV in the energy measurement; ^{*}[TO]: total oxygen content in each glass sample.

is kept constant for all glasses and therefore we would expect the NBO percentage to be constant. The peak position of the fitted spectrum representing oxygen atoms in Si–O–Si and Si–O–Ce configurations, is seen to shift toward lower BE with increase in CeO₂ content (see Table 3). This is due to the increase in oxygen atoms in Si–O–Ce configuration in which the oxygen atoms have a slightly lower BE than those in the configuration Si–O–Si, inducing a decrease in the overall BE of this contribution to the O 1s spectra. We also note that the FWHM of the BO increases from 1.91 eV for $x=0.025$ to 2.21 eV for $x=0.10$. This is due to the fact that the oxygen in the site Si–O–Ce is increasing, contributing to the BO signal with increase in CeO₂ content in the glass. We also note in Fig. 4 that the intensity of the NBO signal at $x=0.10$ is more enhanced than for the other glass compositions. One might think that the NBO contribution has increased compared to the other compositions. We think that the enhancement of the NBO contribution is due to the fact that the FWHM of the BO signal is large while the energy separation between the BO (Si–O–Si and Si–O–Ce) and NBO (Si–O–Na⁺) peaks is small for that composition (see Table 3). The calculated values of the proportion of NBO in the glass based on the fact that each Na₂O introduces two NBO's are reported in Table 3 and has a value close to 35% for all glass compositions. The measured NBO content based on the two peak fits of the O 1s core level spectra is also reported in Table 3. There is good agreement between the measured and the calculated values indicating that Ce ions behave more like a glass intermediate introducing BO. It is not possible with the present resolution of our XPS instrument to resolve experimentally the three contributions to the O 1s spectra and therefore impossible to determine experimentally the number of Si–O–Ce sites in these glasses.

4. Conclusion

The physical and structural properties of CeO₂–Na₂O–SiO₂ glass series were investigated. The physical properties measurements indicate that introducing Ce ions in the glass strengthen its network structure as seen by the increase in T_g and α . An XPS analysis of the Ce oxidation state reveals that Ce(III) ions are predominant for the three glasses compositions with $x \leq 0.075$, while a mixed

valence glass was found for the composition $x=0.10$. The O 1s core level spectra were fitted with two contributions, BO and NBO. The BO contribution was found to increase with increase in CeO₂ content indicating the Ce ions enter the glass network as glass intermediate for all compositions investigated in this study.

Acknowledgments

The author would like to acknowledge the support of Physics Department at KFUPM and the Research Institute at KFUPM for the ICP measurements. I also thank Dr. D. Holland at Warwick University for providing the sample preparation and the thermal measurements facilities.

References

- [1] K. Machida, J. Ceram. Soc. Jpn. 111 (2003) 162.
- [2] N. Tang, B. Fuquan, J.L. Wang, X.Y. Yin, G.H. Wu, F.M. Yang, Z.M. Chen, G.C. Hadjipanayis, IEEE Trans. Magn. 37 (2001) 2546.
- [3] A.T. Pedziwiatr, B.F. Bogacz, R. Gargula, S. Wrobel, J. Magn. Mater. 248 (2002) 19.
- [4] Z. Hui, P. Michele, J. Mater. Chem. 12 (2002) 3787.
- [5] K. Annapurna, R.N. Dwivedi, P. Kundu, S. Buddhudu, Mater. Lett. 58 (2004) 787.
- [6] F.B. Noronha, E.C. Fendley, R.S. Soares, W.E. Alvares, D.E. Resasco, Chem. Eng. J. 82 (2001) 21.
- [7] U. Caldino, J. Phys. Cond. Mater. 15 (2003) 7127.
- [8] A. Kucuk, C. Alexis, Opt. Mater. 13 (1999) 279.
- [9] M.A. Garcia, J. Llopis, M.A. Villegas, S.E. Paje, J. Alloys Compd. 323 (2001) 367.
- [10] A. Vedda, A. Baraldi, C. Canevali, R. Capelletti, N. Chiodini, R. Francini, M. Martini, F. Morazzoni, M. Nikl, R. Scotti, G. Spinolo, Nucl. Inst. Methods A 486 (2002) 259.
- [11] G.K. Das Mohapatra, Phys. Chem. Glasses 40 (1999) 12.
- [12] B.M. Reddy, A. Khan, Y. Yamada, T. Kobayashi, S. Loridant, J.C. Volta, J. Phys. Chem. B 107 (2003) 11475.
- [13] C.G. Pentano, in: C. Simmons, O. El-Bayoumi (Eds.), Experiments in Glass Science, American Ceramic Society, Westerville, Ohio, 1993 (Chapter 5).
- [14] A. Mekki, K. Ziq, D. Holland, C.F. McConville, Phys. Chem. Glasses 43 (2002) 41.
- [15] P.G. Harrison, J.W. Wood, A. Kelsall, Phys. Chem. Glasses 41 (2000) 165.
- [16] S. Gavarini, M.J. Guittet, P. Trocellier, M. Gauthier-Soyer, F. Carrot, G. Matzen, J. Nucl. Mater. 322 (2003) 111.
- [17] D.A. Creaser, P.G. Harrison, M.A. Morris, B.A. Wolfendale, Catal. Lett. 23 (1994) 13.

- [18] F. Larachi, J. Pierre, A. Adnot, A. Bernis, *Appl. Surf. Sci.* 195 (2002) 236.
- [19] P. Burroughs, A. Hamnett, A.F. Orchard, G. Thornton, *Chem. Soc. Dalton Trans.* 17 (1976) 1686.
- [20] D. Holland, I.A. Gee, A. Mekki, C.F. McConville, *Phys. Chem. Glasses* 42 (2001) 247.
- [21] R. Bruckner, H.U. Chun, H. Goretzki, M. Sammet, *J. Non-Cryst. Solids* 42 (1980) 49.